Proceedings of the ASME 2024 19th International Manufacturing Science and Engineering Conference
MSEC2024
June 17 – June 21, 2024, Knoxville, Tennessee

MSEC2024-125340

MANUFACTURING CATHODES VIA DRY-PROCESSING FOR LITHIUM-ION BATTERIES

Runming Tao
Electrification and Energy Infrastructures Division, Oak Ridge National Laboratory
Oak Ridge, TN, USA

Bryan Steinhoff
Navitas Systems LLC
Ann Arbor, MI, USA

Yang-Tse Cheng
Chemical and Materials Engineering, University of Kentucky, Lexington, KY, USA

Jianlin Li*
Applied Materials Division, Argonne National Laboratory
Lemont, IL, USA

ABSTRACT

Conventional lithium-ion battery (LIB) electrodes are prepared through a wet slurry process with n-methyl pyrrolidone solvent, especially for cathodes. The wet slurry process encounters several disadvantages such as binder migration, electrode cracking in thick electrodes, energy intense heat-dry NMP solvent removal, and costly NMP recovery. The cost and energy consumption of coating and drying of electrode are about 11.5 % and >46 % in LIB manufacturing, respectively. Thereby, it is essential to develop a facile roll-to-roll solvent-free LIB electrode processing for reducing the cost and energy consumption.

Recently, the Maxwell-type dry processing (DP) shines new lights on LIB manufacturing, which mainly bases on dry mixing (DM) of electrode component powder followed by calendering into electrode films and laminating onto current collectors, realizing the rapid manufacturing of LIB electrodes in a powder-to-film manner for industries. This report shares some recent progress on the DP from our group. We aim to further advance the manufacturing science of DP by correlating the processing conditions with electrode properties and performance. Particularly, we investigate the effect of DM, and compression on the polytetrafluoroethylene (PTFE) binder fiberization, porosity, mechanical properties, electrical conductivity and electrochemical behaviors of electrodes.

The DM study suggests that PTFE fiberization heavily relies on the degree of DM. Insufficient DM results in poor PTFE fiberization while outrageous DM damages the formed PTFE fibers. Both negatively affect the mechanical behaviors of the electrodes and its rate capability. However, moderate DM is highly beneficial. In addition, our study of the porosity impact reveals that $LiNi_{0.8}Mn_{0.1}Co_{0.1}O_2$ (NMC) secondary particles can be broken into primary particles due to compression, especially at low porosity. Those fractured NMC secondary particles exhibits lower modulus. We propose that a moderate porosity of around 32% favors the electronic conductivity, charge transfer impedance and rate capability. The study of the cathodic electrolyte interphase layer of PTFE-based DPed electrode confirms that side reactions of PTFE binder due to the formation of LiF in $LiClO_4$-based electrolyte.

Keywords: Dry processing, Lithium-ion batteries, Energy density, Sustainable manufacturing, Dry mixing, Porosity

NOMENCLATURE

DP	dry processing
DPEs	dry-processed electrodes
LIBs	lithium-ion batteries
NMP	n-methyl pyrrolidone
NMC811	$LiNi_{0.8}Mn_{0.1}Co_{0.1}O_2$
NMC622	$LiNi_{0.6}Mn_{0.2}Co_{0.2}O_2$
DM	dry mixing
PTFE	polytetrafluoroethylene
EIS	electrochemical impedance spectroscopy
SEM	scanning electron microscope
XPS	X-ray photoelectron spectroscopy
CEI	cathodic electrolyte interphase
TEM	transmission electron microscope

1. INTRODUCTION

Lithium-ion batteries (LIBs) are promising for electric vehicles.[1] Currently, LIBs are based on conventional electrodes that are prepared by roll-to-roll wet slurry processing methods. Unfortunately, this route is time- and energy-consuming due to the involved slurry preparation, coater slurry casting, and slurry heat drying, which leads to ~11.5 % of manufacturing costs and >46 % energy consumption in LIB manufacturing.[2] It is also important to note that for LIB cathodes, owing to the high toxicity of n-methyl pyrrolidone (NMP) solvent, a costly solvent recovery is needed as well, which requires pricy equipment with energy-intense operation.

Additionally, the conventional wet processing cannot fulfill high-loading EV electrodes. This is mainly due to the binder migration issues rooted in heat drying, namely, limited mechanical strength, non-uniform distribution of electrode component materials, and poor rate capability. Therefore, developing dry processing (or solvent-free processing) is essential for large-scale manufacturing of high-loading cathodes for EVs.

Meanwhile, Maxwell Technologies Inc. developed an electrode dry processing (DP) route for commercial capacitors and/or supercapacitors.[3] Recently, Tesla purchased 55 % premium of Maxwell Technologies Inc for its DP strategy and practiced the DP in EV LIB cathode manufacturing in 2020.[4] Typically, as the scheme exhibited in Figure 1, the Maxwell-type DP involves three major steps: 1) dry mixing (DM) of active material, polytetrafluoroethylene (PTFE) binder, and conductive carbon black, which not only homogenize those electrode component materials in a short timeframe, but also applies high shearing to pre-fiberize the PTFE binder, 2) calendering the DMed powder mixture into a free-standing electrode film, and 3) laminating the free-standing electrode film onto a current collector.[5] However, few details and achievements of DP and/or dry-processed electrodes (DPEs) have been reported in literature. Moreover, the impact of DP on electrode structure, electrochemical performance and cathodic electrolyte interphase (CEI) layer is barely reported. Therefore, establishing fundamental understanding of DP is of-interest for advanced manufacturing of LIBs.

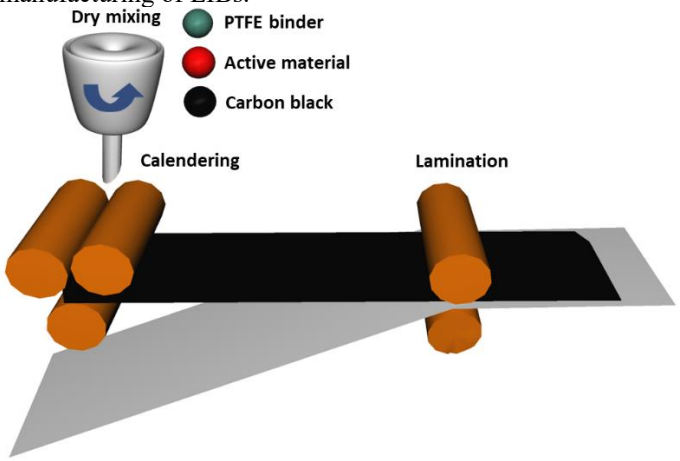

Figure 1: Schematic demonstration of the DP strategy. Reproduced from reference 8 with permission from Elsevier, Copyright 2023.

Herein, this conference proceeding article discusses some of our recent achievements and discovery of DP. The first part of this paper discusses our study of the impact of DM on the powder mixture properties, electrode structure, and electrochemical performance. It is suggested that a moderate degree of DM can favors the DPE performance in LIB cells. In the second part, the porosity effects on DPEs are probed, revealing that DPE with a moderate porosity of 32 % exhibits desirable electrochemical performance due to its low charge transfer impedance and good electronic conductivity.

2. MATERIALS AND METHODS

The $LiNi_{0.6}Mn_{0.2}Co_{0.2}O_2$ (NMC622) and $LiNi_{0.6}Mn_{0.2}Co_{0.2}O_2$ (NMC811) were purchased from Targray. The conductive carbon was acquired from Cabot Corporation. The PTFE powder was purchased from Chemours. Gen 2 electrolyte was purchased from Tomiyama Pure Chemical Industries LTD, which contains 1.2 M of $LiPF_6$ in ethylene carbonate and ethylmethyl carbonate with a weight ratio of 3:7. All the chemicals were directly used as received, and no further treatment was performed to the chemicals.

2.1 Ball mill-based DP

92 wt.% of NMC622, 3 wt.% carbon black and 5 wt.% PTFE were DMed on a ball mill (Retsch MM400) for 10, 30, or 60 min at a constant vibrational frequency of 30 Hz. The resulting powder mixtures were calendered into free-standing electrode films. Consecutively, they were laminated onto carbon-coated aluminum foils. The delivered DPEs had a NMC622 loading of ~40.0 mg cm^{-2} (~7.2 mAh cm^{-2}) and a thickness of ~153 µm. Based on the DM time, the DPEs were denoted as DPE-10, DPE-30 and DPE-60, respectively.

2.2 High-energy twin-screw extruder

92 wt.% of NMC811, 3 wt.% carbon black and 5 wt.% PTFE were DMed on a 20-mm high-energy twin-screw extruder (Bühler Group, Switzerland) at a feed rate of 1.5 kg h^{-1}. The resulted powder mixture was calendered into a free-standing electrode film. Finally, the obtained free-standing electrode film was laminated onto a carbon-coated aluminum foil. The delivered DPEs had a NMC811 loading of 33.0 mg cm^{-2} (~6.6 mAh cm^{-2}) with porosity of 22, 32, and 39 %, which are denoted as 22%-DPE, 32%-DPE, and 39%-DPE, respectively. The porosity of DPEs was calculated via the following equation,

$$\varepsilon = 1 - \frac{m_{areal}}{L}\left(\frac{\omega_{AM}}{\rho_{AM}} + \frac{\omega_B}{\rho_B} + \frac{\omega_{CA}}{\rho_{CA}}\right) \quad (1)$$

, where ε, m_{areal}, L, ρ and ω are the porosity, the areal mass loading, the electrode coating thickness, the electrode component densities and the mass fractions, respectively.[6, 7]

2.3 Typical characterizations

Scanning electron microscope (SEM) study was carried out on a Zeiss Merlin VP. The mechanical strength was tested on a MicroMaterials NanoTest Vantage micro indenter. The load-controlled tests were performed using a diamond Berkovich indenter with a maximum load of 150 mN. For each DPE sample, 20 measurements were taken in 4 × 5 arrays with 600 µm spacing between each indent. The sheet resistance data of the DPEs was obtained on a four-point probe (Ossila Ltd, Sheffield, UK). X-ray photoelectron spectroscopy (XPS) study was conducted on a Thermo Scientific X-ray photoelectron spectrometer with a monochromated Al K_α (1486.6 eV) X-ray source focused to a 400-micron spot under a pressure below 1×10^{-7} mbar. The XPS data analysis was based on Thermo Scientific Avantage v.5.966 software. Transmission electron microscope (TEM) images were collected on a JEOL JEM-2100F and/or a Thermo Scientific

(formerly FEI) Titan Themis G2 200 probe Cs-corrected TEM at 200 kV.

2.4 Electrochemical performance study

CR2032-type coin cells were assembled in an argon-filled glovebox with oxygen and moisture contents less than 0.1 ppm. Celgard 2325 and lithium metal were used as the separator and counter electrode, respectively.

Charge/discharge tests were carried out on a Maccor Series 4000 tester. The test protocol is based on constant-current charge with subsequent constant-voltage charge (at 4.3 V) followed by constant current discharge in a voltage range of 3.0 – 4.3 V. At 1C, current densities of NMC622 and NMC811 DPEs were set at 180 and 200 mA g^{-1}, respectively. The electrochemical impedance spectra (EIS) were collected from a BioLogic VSP3 system at an amplitude of 10 mV in a frequency range of 10 mHz – 600 kHz, which was then fitted by the ZFit tool in EC-Lab V11.43 software.

3. RESULTS AND DISCUSSION

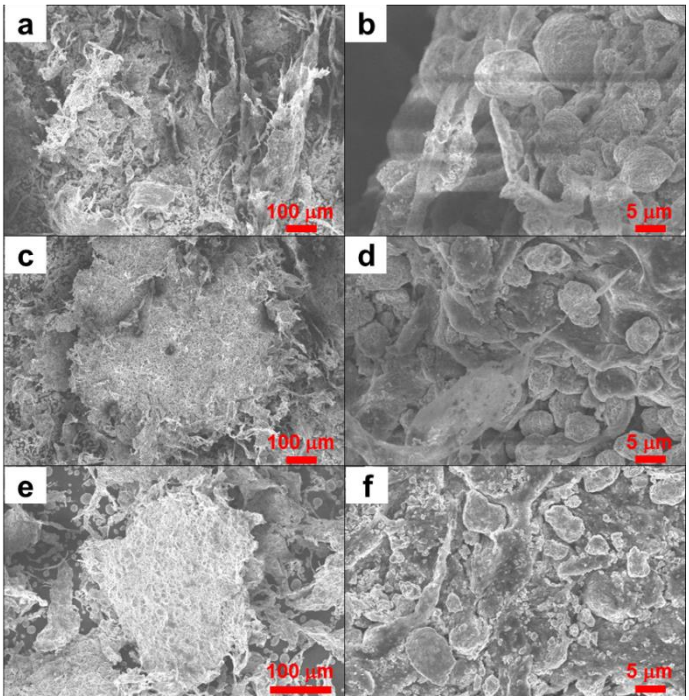

FIGURE 2: SEM images of DMed powder mixtures with various degree of DM at low and high magnifications, (a and b) DPE-10, (c and d) DPE-30, (e and f) DPE-60, respectively. Reproduced from reference 8 with permission from Elsevier, Copyright 2023.

In one of our recent DP papers,[8] to probe to the effects of DM on the powder mixture, PTFE fiberization, DPE structure, and DPE LIB performance, electrode components were DMed on a ball mill for different time durations, delivering three DPEs with different degree of DM. Different degrees of DM indeed cause huge differences in the morphology and structure of DPE powder mixture. As the SEM images shown in Figure 2a below, for the powder mixture of DPE-10, majority of PTFE is slightly fiberized, and the homogeneity of those electrode component materials is poor. Figure 2b presents that small broken NMC primary particle can be observed. This indicates the low degree of DM does not affect the structure integrity of NMC active material. At a moderate degree of DM (Figure 2c), the powder mixture of DPE-30 exhibits flake-like morphology with the evenly distributed NMC active material. As displayed in Figure 2d, obvious PTFE fibers and NMC secondary particles are observed. These results suggest that moderate degree of DM has little impact on NMC morphology and can integrate NMC and conductive carbon black via the binding effect of PTFE fibers. Further increasing the degree of DM (Figure 2e and 2f), although the flake-like morphology of DPE-60 powder mixture can still be detected, considerable amount of NMC material is broken into primary particles, causing huge NMC particle size distribution, which is not favorable for the electrochemical kinetics in LIBs. Additionally, it is worth noting that the excessive DM can damage the formed PTFE fibers, reducing the mechanical strength of the DPE. According to the aforementioned SEM study, it is believed that moderate degree of DM is more desirable for enhancing the electrochemical performance of DPE in LIBs.

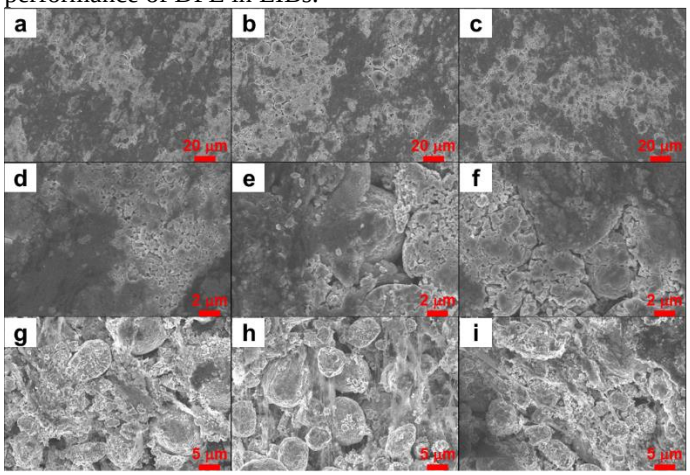

FIGURE 3: (a – c) Low-magnification top-view SEM images of DPE-10, DPE-30 and DPE-60, respectively. (d – e) High-magnification top-view SEM images of DPE-10, DPE-30 and DPE-60, respectively. (g – i) Cross-sectional SEM images of DPE-10, DPE-30 and DPE-60, respectively. Reproduced from reference 8 with permission from Elsevier, Copyright 2023.

As the SEM images shown in Figure 3a – 3f, owing to the huge compression and shearing force during calendering and lamination, which breaks NMC secondary particles into NMC primary particles, the surface morphology of DPEs with various degree of DM is highly comparable, exhibiting abundant NMC primary particles and obvious localized carbon-NMC segregation. However, the cross-sectional SEM images in Figure 3g – 3i indicate obvious difference in the internal structures of those DPEs. Notably, DPE-30 exhibits abundant PTFE fibers, which is in line with the structural feature of the corresponding powder mixtures.

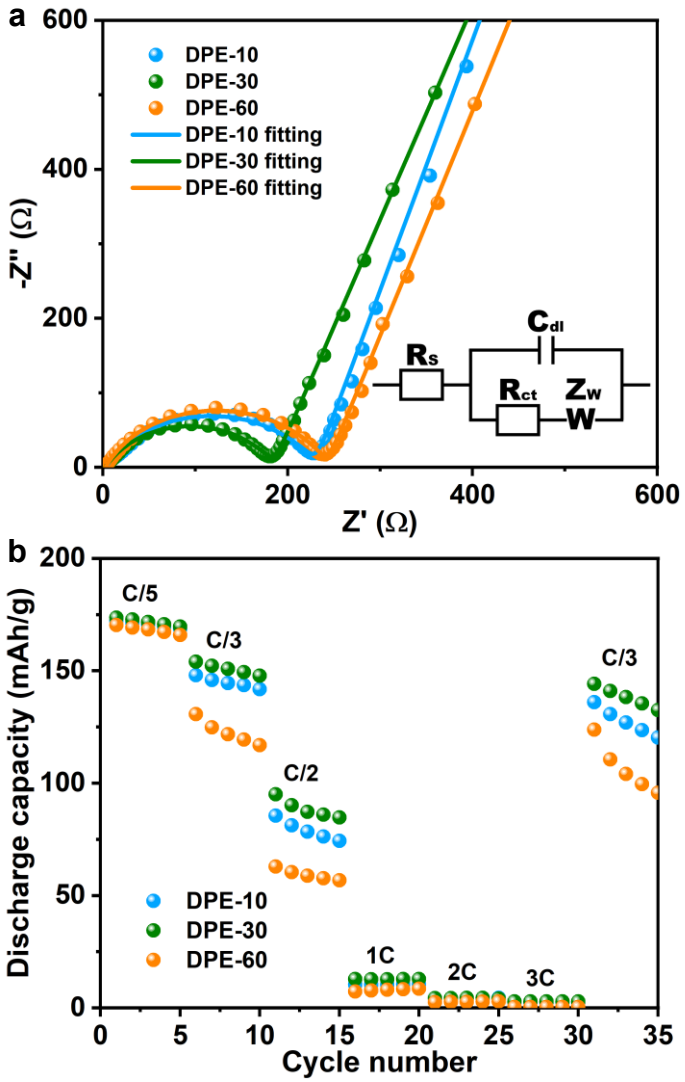

Figure 4: (a) EIS Nyquist plots and (b) rate performance of DPEs with various DM time. Reproduced from reference 8 with permission from Elsevier, Copyright 2023.

The EIS data of DPEs in Figure 4a features the typical Randles circuit. In the high and low frequency regions, the three DPEs exhibit comparable systemic impedance (R_s) and Warburg impedance (Z_W), respectively.[9] However, DPE-30 presents considerably smaller charge transfer impedance (R_{ct}) than the rest two DPE do in the mid-high frequency region.[10] Such observation is rooted in the moderate degree of DM, which ensures the uniformity of electrode component materials and the integrity of NMC secondary particles for fast electrochemical kinetics. Thus, it can be speculated from EIS that the order of electrochemical kinetics for those three DPEs is DPE-30>DPE-10>DPE-60. Indeed, the rate performance of the three DPEs in Figure 4b follows the aforementioned order. Such observations reveal that the degree of DM has huge impact on the structure of DPE and its R_{ct} value.

In our recent study of compression effects on DPEs,[11] porosity of DPE was applied to monitor the degree of compression. As the cross-sectional SEM images shown in Figure 5, those cross-sectional SEM images display a thin and dense layer at the top surface region and a thick and porous layer below. Abundant NMC secondary particles appear in the bottom region, while the top layer only exhibits fine NMC primary particles. Indeed, the top-view SEM images further verify the appearance of fractured small NMC primary particles. Such bi-layered structure of DPEs is potentially attributed to the high shearing force on the top surface during the lamination step in DP.

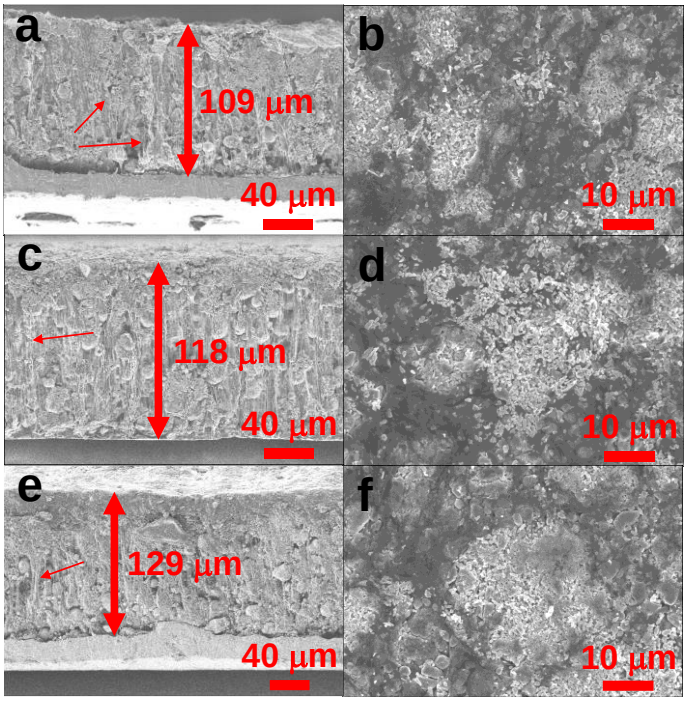

FIGURE 5: Cross-sectional and top-view SEM images of DPEs with porosity of (a and b) 22%-DPE, (c and d) 32%-DPE and (e and f) 39%-DPE, respectively. The small arrows in (a), (c) and (e) indicate the formed PTFE fibers. Reproduced from reference 11 with permission from Elsevier, Copyright 2023.

As shown in Figure 6a, at small load, DPE with higher porosity exhibits less displacement than that DPE with lower porosity does, vice versa at big load. Furthermore, based on following equations,

$$E_r = \frac{S}{2}\sqrt{\frac{\pi}{A}} \quad (2)$$

$$\frac{1}{E_r} = \frac{1-v_i^2}{E_i} + \frac{1-v_s^2}{E_s} \quad (3)$$

$$H = \frac{P_{max}}{A} \quad (4)$$

, average hardness and modulus were calculated (Figure 5b). Owing to the random distribution of electrode component materials in DPEs, huge variation (standard deviation) is expected. Moreover, it is interesting to note that the measured hardness and modulus of DPEs are much lower than those of NMC particles (e.g., 142.5 ±11.3 GPa modulus and 8.6 ± 1.3 GPa hardness).[12] Such results are probably ascribed to the fracture of NMC secondary particles during DP. Because the

measurements are mainly taken on the thin top surface layer with abundant NMC primary particles.

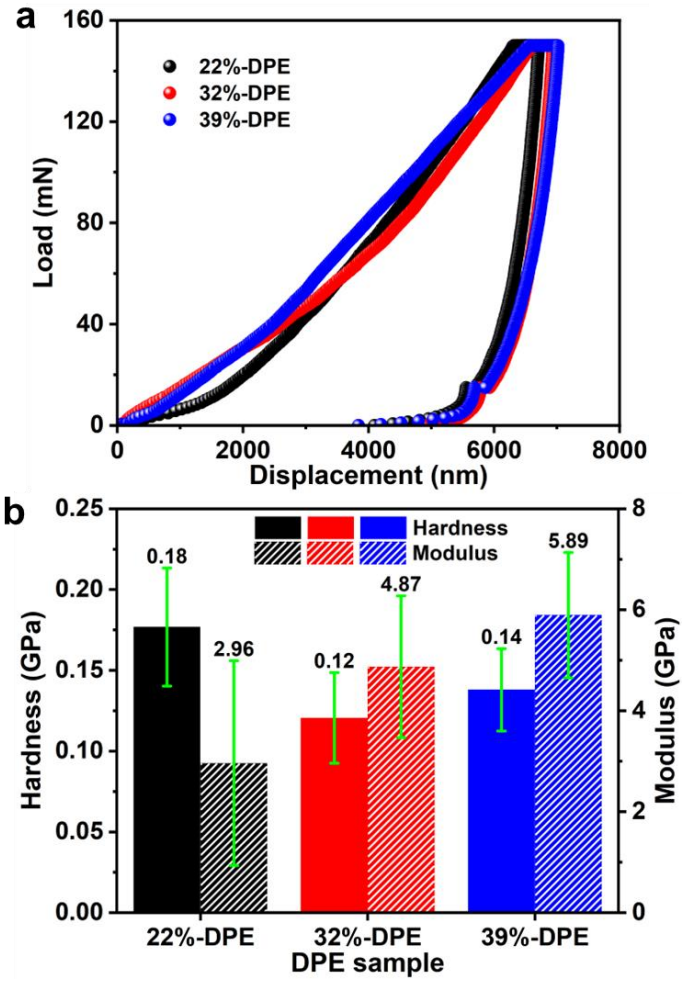

FIGURE 6: Mechanical strength measurements. (a and b) Load Vs. displacement curve and the estimated average hardness and modulus values, respectively. Reproduced from reference 11 with permission from Elsevier, Copyright 2023.

We probed the compression effect on the electronic conductivity of DPEs via four-point probe measurements (Figure 7a). Figure 7b presents that the sheet resistance is in an order of 39%-DPE > 22%-DPE > 32%-DPE. The electrode components in high porosity DPE may not be well connected. At a moderate porosity, the DPE structure is denser, leading to a better percolation network with less sheet resistance. However, low porosity can cause large sheet resistance. This may be rooted in the facture of NMC secondary particles that forms electronically isolated NMC primary particles.

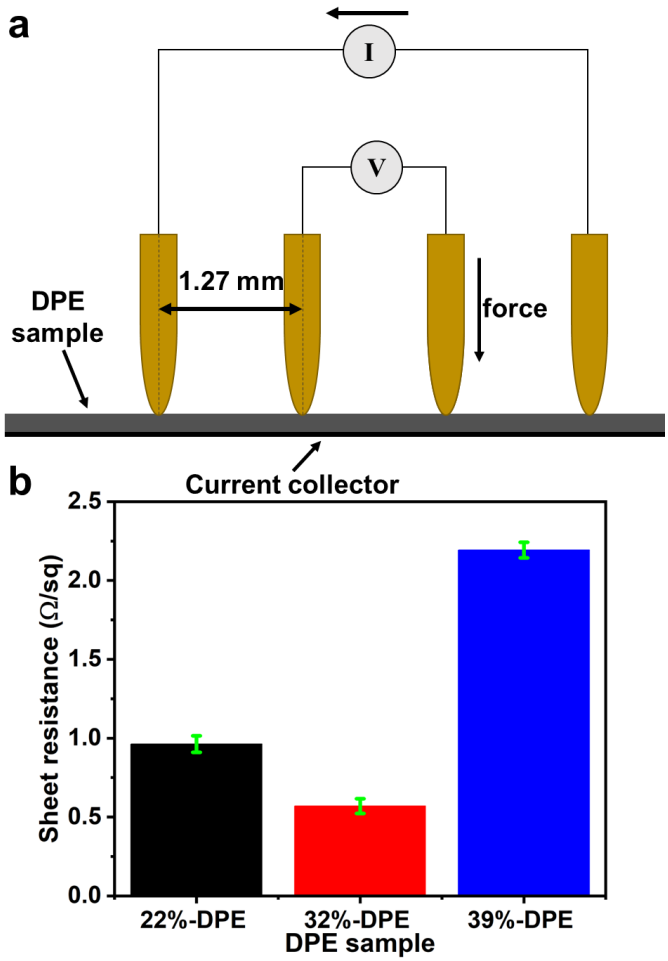

FIGURE 7: Four-point probe electronic conductivity measurements a) schematic demonstration of the four-point problem experiment and b) sheet resistance. Reproduced from reference 11 with permission from Elsevier, Copyright 2023.

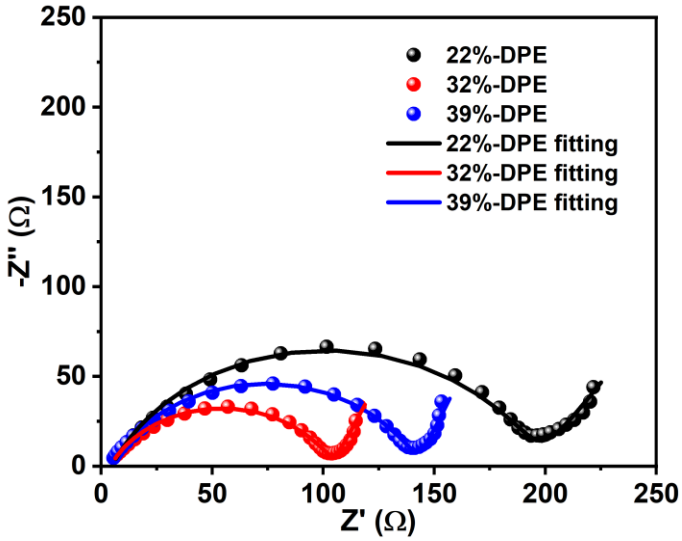

FIGURE 8: EIS Nyquist plots of DPEs with various porosity. Reproduced from reference 11 with permission from Elsevier, Copyright 2023.

The EIS Nyquist plots in Figure 8 suggests that DPE-based half cells feature the typical Randels circuit. Notably, comparable Ohmic impedance is observed, which is not consistent with the results of the four-point probe study above because of the domination of the contact resistance of coin cell parts and/or the resistances of electrolyte and lithium metal. Additionally, 32%-DPE presents the smallest R_{ct} values of the DPEs are in an order of 32%-DPE<39%-DPE<22%-DPE. Typically, DPE with low porosity has limited contact area between electrode and electrolyte limited and electrochemically isolated NMC particles, while high porosity can enlarge the electrode-electrolyte contact area, though, Li^+ diffusion length can be elongated. Fortunately, sufficient void for charge transfer at the electrode-electrolyte interface can be ensured at a porosity of 32%, which has dense enough structure for straightforward Li^+ diffusion pathway as well. Moreover, the steep linear fitting of 32%-DPE in the low frequency region further confirms the fast electrochemical kinetics. As expected, the rate performance test in Figure 9 indicates that 32%-DPE exhibits the best rate capability, especially at current densities of C/2 and 1C. Additionally, 32%-DPE also exhibits the highest electrochemical reversibility at the recovery C/3. Thereby, it can be concluded that moderately compressed DPEs with moderate porosity are beneficial to electrochemical kinetics. Notably, it can be expected that the electrochemical performance of DPEs could be superior to that of conventional electrodes, which is mainly due to the reduced tortuosity and the elimination of binder migration effects.[4, 5] Additionally, for those ultrahigh-loading DPEs, the cycling is generally performed at a small current rate of C/3 or lower, and thereby the cyclability would not be significantly affected by porosity and its resulted electrochemical kinetics.

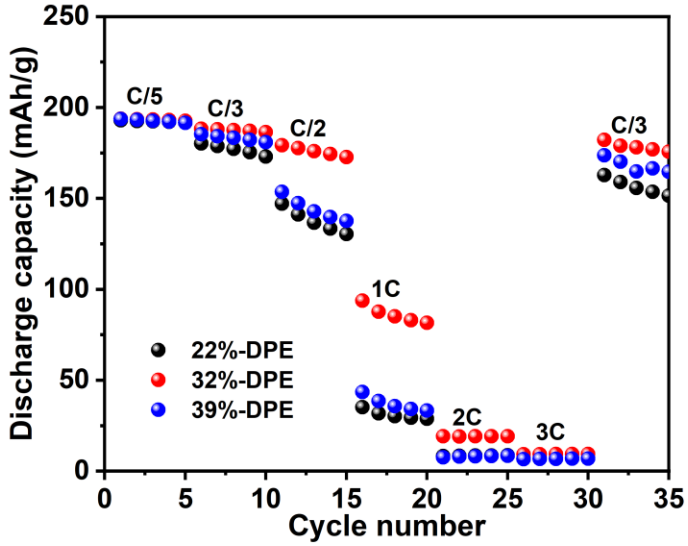

FIGURE 9: rate performance of DPEs with various porosity. Reproduced from reference 11 with permission from Elsevier, Copyright 2023.

As shown in Figure 10, the compression effects on DPEs are summarized into the following aspects. 1) Compression directly dictates porosity of DPEs, which is also relative to the morphology and structure of DPEs. 2) The high shear force during calendering and lamination can also break NMC secondary particles into primary particles. 3) Porosity reflects the contact among electrode component materials and thus may have some influence on the electronic conductivity. 4) Most importantly, all the aforementioned aspects impact the electrochemical kinetics of DPEs in LIB cells. 5) Structure of DPE is related to its mechanical strength as well.

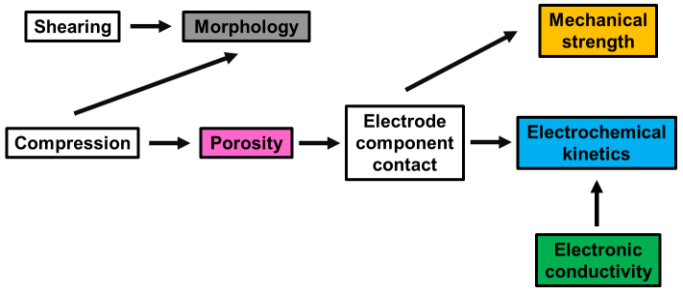

FIGURE 10: schematic demonstration of the impact of porosity for DPEs. Reproduced from reference 11 with permission from Elsevier, Copyright 2023.

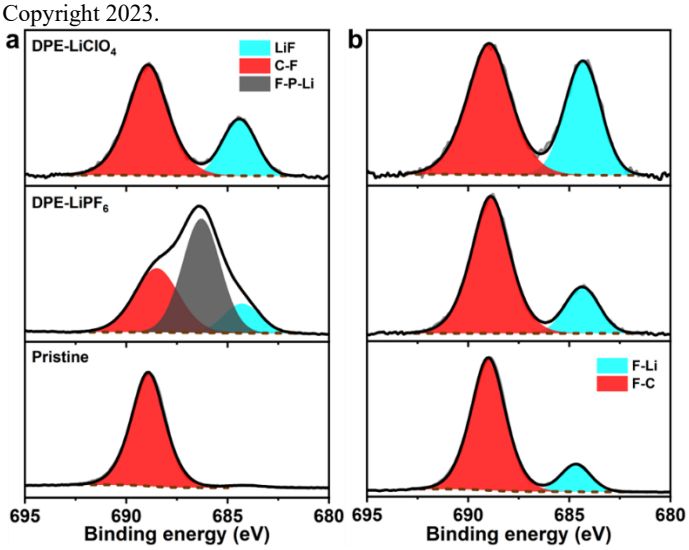

FIGURE 11: HRXPS of F 1s for (a) comparison and (b) three repeating measurements for DPE-$LiClO_4$ samples. Reproduced from reference 13 with permission from American Chemical Society, Copyright 2023.

To probe the electrochemical stability of PTFE binder and the CEI chemistry for dry LIB cathodes, a set of XPS experiments was performed in a recent of our DP work,[13] which involves the typical Gen II electrolyte with $LiPF_6$ and a fluorine-free electrolyte with the identical electrolyte solvent system and $LiClO_4$ salt. The $LiClO_4$-based electrolyte can eliminate the potential fluorine source to illustrate the side reactions of PTFE. As shown in Figure 11a, comparing to the pristine DPE with only C-F signal at 688.9 eV from PTFE binder, the DPEs cycled with $LiPF_6$ and $LiClO_4$ (denoted as DPE-$LiPF_6$ and DPE-$LiClO_4$, respectively) contains strong noticeable LiF signal at 684.4 eV, which directly implies the decomposition of PTFE binder in LIB cathode. Furthermore, to confirm this phenomenon, three additional measurements were

carried out. Indeed, LiF species is observed in the CEI layer of DPE-$LiClO_4$ (Figure 11b). It is worth noting that the concentration of LiF of the four measurements of DPE-$LiClO_4$ are different, which can be attributed to the different X-ray irradiation spots. As shown in Figure 3 and 5, DPE surface contains some NMC-rich area and some carbon- and PTFE-rich area. Additionally, as displayed in Figure 12, no signal of NMC species appears on the HRXPS of DPE-$LiPF_6$, while transition metal signals can be clearly detected on DPE-$LiClO_4$. These results suggest that the thickness of the CEI layer on DPE-$LiClO_4$ is less than that of DPE-$LiPF_6$, which is also confirmed by the TEM study (Figure 13).

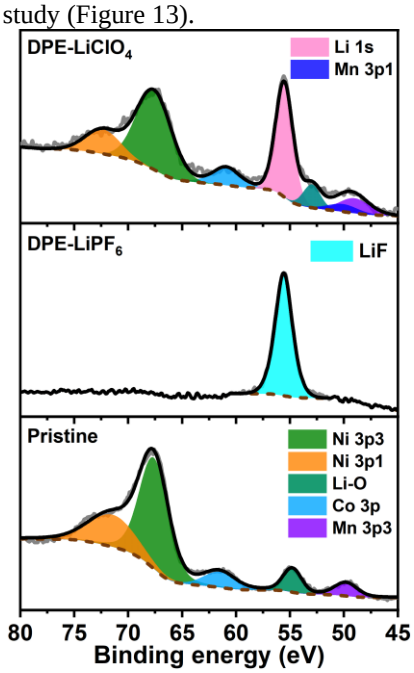

Figure 12: HRXPS of Li 1s. Reproduced from reference 13 with permission from American Chemical Society, Copyright 2023.

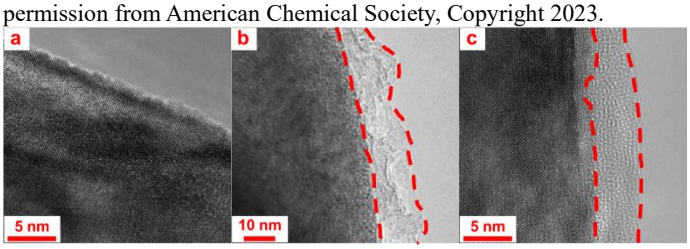

Figure 13: (a – c) TEM images of the pristine, $LiPF_6$-cycled and $LiClO_4$-cycled DPEs, respectively. Reproduced from reference 13 with permission from American Chemical Society, Copyright 2023.

4. CONCLUSION

In summary, our recent work delivers some fundamental understanding of DP for LIB manufacturing. The effects of DM and compression in DP strategy were successfully established, suggesting that moderate degree of DM and moderate compression are more favorable for the LIB electrochemical performance due to the ensured electrochemical kinetics. Furthermore, we would like note that with development of artificial intelligence and machine learning, the understanding of impact of DM and compression may be further enriched via modelling studies to facilitate the optimization in industries. Our study of the properties of the CEI layer on DPEs novelly confirms the side reactions of PTFE binder, which implies more efforts on the engineering of PTFE binder and electrolyte are also needed to optimize the dry LIBs. It is believed that our studies of DP can potentially pave the avenue of future manufacturing of high-performance LIBs.

ACKNOWLEDGEMENTS

This research at Oak Ridge National Laboratory (ORNL), managed by UT Battelle, LLC, for the U.S. Department of Energy (DOE) under contract DE-AC05-00OR22725, was sponsored by the DOE Advanced Manufacturing Office and Advanced Materials & Manufacturing Technologies Office (DE-EE0009109). The SEM characterization was conducted at the Center for Nanophase Materials Sciences at ORNL, which is a DOE Office of Science User Facility. The authors are grateful to the colleagues who had contribution in this project. The authors thank Cabot Corporation and Arkema for their material and technical assistance, respectively. The authors also thank the Journal of Power Sources for approving the copyrights of the contents in this conference proceeding article. The United States Government retains and the publisher, by accepting the article for publication, acknowledges that the United States Government retains a non-exclusive, paid-up, irrevocable, world-wide license to publish or reproduce the published form of this manuscript, or allow others to do so, for United States Government purposes. The DOE will provide public access to these results of federally sponsored research under the DOE Public Access Plan (http://energy.gov/downloads/doe-public-access-plan).

REFERENCES

[1] Goodenough, J. B., 2018, "How We Made the Li-Ion Rechargeable Battery," Nat. Electron., 1(3), pp. 204-204.
[2] Li, J., Fleetwood, J., Hawley, W. B., and Kays, W., 2022, "From Materials to Cell: State-of-the-Art and Prospective Technologies for Lithium-Ion Battery Electrode Processing," Chem. Rev., 122(1), pp. 903-956.
[3] Lu, Y., Zhao, C.-Z., Yuan, H., Hu, J.-K., Huang, J.-Q., and Zhang, Q., 2022, "Dry Electrode Technology, the Rising Star in Solid-State Battery Industrialization," Matter, 5(3), pp. 876-898.
[4] Yao, W., Chouchane, M., Li, W., Bai, S., Liu, Z., Li, L., Chen, A. X., Sayahpour, B., Shimizu, R., Raghavendran, G., Schroeder, M. A., Chen, Y.-T., Tan, D. H. S., Sreenarayanan, B., Waters, C. K., Sichler, A., Gould, B., Kountz, D. J., Lipomi, D. J., Zhang, M., and Meng, Y. S., 2023, "A 5 V-Class Cobalt-Free Battery Cathode With High Loading Enabled by Dry Coating," Energy Environ. Sci., 16(4), pp. 1620-1630.
[5] Tao, R., Steinhoff, B., Sun, X.-G., Sardo, K., Skelly, B., Meyer, H. M., Sawicki, C., Polizos, G., Lyu, X., Du, Z., Yang, J., Hong, K., and Li, J., 2023, "High-Throughput and High-Performance Lithium-Ion Batteries via Dry Processing," Chem. Eng. J., 471, p. 144300.
[6] Parikh, D., Christensen, T., and Li, J., 2020, "Correlating the Influence of Porosity, Tortuosity, and Mass Loading on the

Energy Density of LiNi0.6Mn0.2Co0.2O2 Cathodes under Extreme Fast Charging (XFC) Conditions," J. Power Sources, 474, p. 228601.
[7] Zheng, H., Tan, L., Liu, G., Song, X., and Battaglia, V. S., 2012, "Calendering effects on the physical and electrochemical properties of Li[Ni1/3Mn1/3Co1/3]O2 cathode," J. Power Sources, 208, pp. 52-57.
[8] Tao, R., Steinhoff, B., Sawicki, C. H., Sharma, J., Sardo, K., Bishtawi, A., Gibbs, T., and Li, J., 2023, "Unraveling the Impact of the Degree of Dry Mixing on Dry-Processed Lithium-Ion Battery Electrodes," J. Power Sources, 580, p. 233379.
[9] Liang, J., Wang, Z., Huang, L., Zou, P., Liu, X., Ni, Q., Wang, X., Wang, W., and Tao, R., 2023, "Facile and Tunable Synthesis of Nitrogen-Doped Graphene with Different Microstructures for High-Performance Supercapacitors," ACS Mater. Lett., 5(4), pp. 944-954.
[10] Tao, R., Zhang, T., Sun, X.-G., Do-Thanh, C.-L., and Dai, S., 2023, "Ionothermally Synthesized Nanoporous Ti0.95W0.05Nb2O7: a Novel Anode Material for High-Performance Lithium-Ion Batteries," Batteries & Supercaps, 6(6), p. e202300101.
[11] Tao, R., Steinhoff, B., Uzun, K., La Riviere, B., Sardo, K., Skelly, B., Hill, R., Cheng, Y.-T., and Li, J., 2023, "Correlation among Porosity, Mechanical Properties, Morphology, Electronic Conductivity and Electrochemical Kinetics of Dry-Processed Electrodes," J. Power Sources, 581, p. 233481.
[12] Xu, R., Sun, H., de Vasconcelos, L. S., and Zhao, K., 2017, "Mechanical and structural degradation of LiNixMnyCozO2 cathode in Li-ion batteries: an experimental study," J. Electrochem. Soc., 164(13), p. A3333.
[13] Tao, R., Tan, S., Meyer III, H. M., Sun, X.-G., Steinhoff, B., Sardo, K., Bishtawi, A., Gibbs, T., and Li, J., 2023, "Insights into the Chemistry of the Cathodic Electrolyte Interphase for PTFE-Based Dry-Processed Cathodes," ACS Appl. Mater. Interfaces, 15(34), pp. 40488–40495.